Enhanced electrochemical performance of activated carbon derived from *Acacia catechu* bark by KOH activation for supercapacitor application

Pawan Kumar Mishra[1,2,3], *Sabin* Aryal[2], *Hari* Bhakta Oli[2], *Timila* Shrestha[2], *Thakur* Sapkota[4], *Ram* Lal (Swagat) Shrestha[2*], *Deval* Prasad Bhattarai[2*]

[1]Department of Chemistry, Tri Chandra Multiple Campus, Tribhuvan University, Kathmandu, Nepal
[2]Department of Chemistry, Amrit Campus, Tribhuvan University, Kathmandu, Nepal
[3]Central Department of Chemistry, Kirtipur, Tribhuvan University, Kathmandu Nepal
[4]Department of Applied Science and Technology, North Carolina S&T state University, USA

Abstract. The compelling necessity for sustainable energy storage solutions has propelled the advancement of high-performance energy storage strategies. Conventional carbon materials derived from fossils sources cause the limitations of being high rate, processing challenges, and potential harm. Conversely, activated carbon sourced from biomass has emerged as a promising substitute due to its abundant presence in nature, high carbon content, and ease of processing with minimal toxicity. This study outlines the production of activated carbon from the matured bark of Acacia catechu through a sequence of processes, including pre-carbonization, carbonization, and activation at varying temperatures utilizing potassium hydroxide (KOH) as an activating agent. The prepared specimen underwent analysis using diverse methods such as iodine and methylene blue number techniques, XRD, FTIR-test, Raman test, TEM, and its potential storage capacity was appraised via CV, GCD, EIS, and CV stability tests paying a three-electrode arrangement. The activated carbon synthesized at 800 °C (KBAC-8) demonstrated a specific capacitance of 264.51 F/g at 1 A/g, with outstanding retention of 94.64% and superior coulombic efficiency equated to KBAC-6 and KBAC-4. Overall results suggest the relevance of KBAC-8 for supercapacitor applications due to its subordinate resistance.

1 Introduction

Biomass, as an abundant and renewable resource, has become a focal point in the design of sustainable precursors-based carbonaceous materials tailored for energy storage systems [1]. Global biomass reserves are estimated at approximately 55 billion metric tons of carbon in a desiccated state, with the majority originating from vegetative sources, totaling around 45 billion tons [2]. The transition towards sustainable energy solutions has prompted the exploration of eco-friendly and efficient conversion methods to transform biomass into high-performance carbon materials. This shift not only addresses greenhouse gas emanations by dropping dependence on relic fuels but also contributes to carbon sequestration, aiding in global climate improvement [3]. One promising derivative of biomass is biomass-derived activated carbon, structurally complex and porous solid rich in carbon content. This material is obtained through the thermochemical degradation of biomass at elevated temperatures in nitrogen atmosphere, typically during moderate carbonization levels [4]. The unique structural and chemical characteristics of biomass-derived activated carbon, including its hierarchical porosity, diverse functional groups and abundant ion-binding sites, make it a suitable material for energy harvesting [5].

In the quest for sustainable and high-performance supercapacitor electrodes, activated carbon derived from biomass emerges as a promising material for energy storage applications [6]. With its elevated surface area, tunable porous configuration, and excellent electrical conductivity, activated carbon is an ideal candidate for supercapacitor materials, striking a balance between energy storage capacity and power delivery [7–9]. Supercapacitors, which are recognized for their high-power density, quick charge and discharge ratios, and extended operational lifetimes, have become the industry standard for energy storage devices. These devices are designed to meet diverse energy storage and release requirements effectively [10]. Despite their advantages, the widespread adoption of supercapacitors is hindered by their relatively modest energy density and the high manufacturing costs involved [11]. The energy storage ability of a supercapacitor is based on various factors, including the composition of electrode materials, electrolyte composition, the interaction

* Corresponding author: swagatstha@gmail.com, devalprasadbhattarai@gmail.com

© The Authors, published by EDP Sciences. This is an open access article distributed under the terms of the Creative Commons Attribution License 4.0 (https://creativecommons.org/licenses/by/4.0/).

between the electrode as well as electrolyte, the overall assembly process, and environmental conditions.

The materials of electrode and their arrangement are among the most important parameters that affect the supercapacitor's electrochemical performance [12]. The composition of the electrode material determines the kind of supercapacitor, which can be either a hybrid, pseudocapacitor, or electrochemical double-layer capacitor (EDLC) [13]. Electrostatic interactions allow EDLC electrode materials, including graphene, carbon nanotubes (CNTs), and activated carbons, to store energy [14]. In contrast, pseudocapacitors utilize materials like conducting polymers and transition metal oxides/phosphides/sulfides that store energy through Faradaic reactions [15]. Hybrid supercapacitors combine the properties of EDLC materials with those of pseudocapacitive or battery-type materials to enhance overall performance [16]. Despite their enhanced capacitance and energy density, pseudocapacitors and hybrid supercapacitors face challenges related to cyclic stability and rate capability [13]. Additionally, the production and disposal of pseudocapacitive and hybrid materials may pose health risks due to the use of transition metals or their composites. So they are precedence by higher stability and environmentally friendly nature of EDLCs [17].

The activation of biomass materials is crucial for unlocking fundamental properties such as high surface area and porosity. There are primarily two methods for activating biomass: physical and chemical stimulation [18]. Physical instigation involves imperiling bio-waste materials to high temperatures in an inert atmosphere. In contrast, chemical activation entails impregnating biomass with activators like phosphoric acid (H_3PO_4), potassium hydroxide (KOH), zinc chloride ($ZnCl_2$), and sodium carbonate (Na_2CO_3), followed by carbonization at specific temperatures [19]. Chemical activation, in particular, is known for its ability to effectively enhance porosity, resulting in a highly porous carbon structure superior to that achieved through physical activation [20].

Acacia catechu (Khair), a native species to South Asia, including Nepal, has been identified as an auspicious precursor intended for creating high-value active carbon because of its abundant bark production and maximum carbon content [21]. The bark of *Acacia catechu*, typically regarded as agricultural waste, can be valorized into high-value AC through the application of appropriate chemical activation processes [22]. The use of potassium hydroxide (KOH) as an activating agent is preferred due to its dehydrating properties, which significantly promote the development of a porous structure. The creation of nanoporous carbon material with a higher surface area involves the impregnation of the precursor materials with KOH, followed by carbonization under inert atmosphere [23].

In this study, *Acacia catechu* bark was utilized as a precursor to synthesize activated carbon at temperatures of 400, 600 and 800 °C. The bark's high lignocellulosic content was leveraged to produce hierarchical nanoporous carbon. The activated carbon derived through the combined physical and chemical process demonstrated optimal supercapacitive performance at the temperature of 800 °C. KOH having 3 M concentration was used as an electrolyte in a three-electrode setup to assess the samples' electrochemical performance. *Acacia catechu* bark-derived activated carbon with potassium hydroxide activation at 800 °C (KBAC-8) revealed a greater gravimetric capacitance of 264.51 F g^{-1} at 1 A g^{-1}, accompanied by a higher degree of micro and mesoporous surface. The lower resistive behaviour of KBAC-8 also contributed to its superior supercapacitive performance. The augmented capacitance of KBAC-8 can be accredited to the manifestation of micropores and mesopores on the surface of the active material, which facilitated electrolyte ion diffusion and enhanced electrochemical performance. The hierarchical nanoporous structure of KBAC-8 allowed for efficient ion transport and storage, resulting in improved supercapacitive performance.

2 Materials and methods

2.1 Materials and preparation

2.1.1 Collection and pre-carbonization of precursor

Acacia catechu bark was collected from the Garambesi, Rainas-7, Lumjung district in Nepal during June, 2021. The bark was reduced to tiny fragments and subjected to shade drying for two months. Subsequently, the dried material was ground into a fine powder using an Herbal Medicine Disintegrator (FW 177) located at Amrit Campus and sieved using a mesh (90 micron) to ensure the consistency of the particulate size. The resulting fine powder of *Acacia catechu* bark was then reserved for the pre-carbonization process. A quantity of 40 grams of the finely powdered bark material was accurately weighed using a digital balance. This powder was sited in a silicon basin and introduced into a muffle kiln, and heated at 250 °C for three hours. The materials obtained after this process are termed as "pre-carbonized precursors" and labelled as KBAC-0.

2.1.2 Activation and Carbonization of the Material

For the activation process, 10 grams of the pre-carbonized bark powder was thoroughly mixed with an equimolar amount of potassium hydroxide. The mixture was pestled using an agate mortar for three hours to create a fine paste. This paste was then transferred to a ceramic boat and allowed to rest at ambient temperature for 24 hours, which was then activated at varying temperature of 400 °C, 600 °C and 800 °C under a Nitrogen (N_2) atmosphere. After the carbonization, the material was once again smashed in an agate mortar to attain a homogeneous mixture. The subsequent mixture was taken in a 250 mL beaker, with the addition of 10 mL of 1 M hydrochloric acid, then 150 mL of distilled water. The suspension was agitated at a speed of 450 rpm for 10 minutes using a magnetic stirrer. The solution was then subjected to repeatedly washing with distilled water till a neutralization condition was accomplished. The solid residue was dried in a hot air

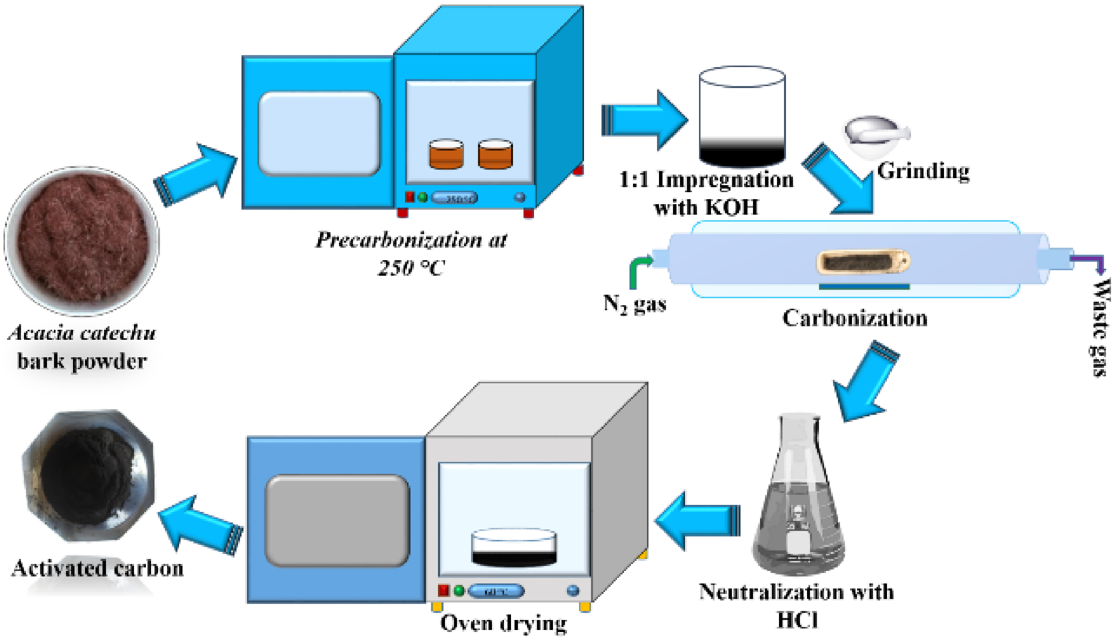

Fig. 1. Schematic diagram representing synthesis of activated carbon from *Acacia catechu* bark using KOH.

oven at 80 °C for 12 hours, followed by vacuum desiccating at 80 °C for an additional 6 hour**.** The dried material was then ground in an agate mortar to obtain a fine powder suitable for characterization**.** The activated carbon samples, synthesized at carbonization temperatures of 400 °C, 600 °C, and 800 °C were designated as KBAC-4, KBAC-6, and KBAC-8, correspondingly**.** A demonstrative illustration of the inclusive process is presented in Fig**.** 1**.**

2.1.3 Electrode preparation

For the preparation of the working electrode, a mixture of 0.5 mg of binder Polyvinylidene fluoride (PVDF) and 0.5 mg of acetylene carbon black was agitated in an agate mortar. To this mixture, 4 mg of the activated carbon was added and then again ground to form a consistent mixture, then subjected onto the nickel foam (1×1 cm^2) using propan-2-ol as a dispersant by drop casting method. The coated nickel foam was dried at 80 °C for 12 hours, resulting in an active mass loading of 3 mg.

2.2 Materials characterization

The activated carbon samples based on KOH underwent analysis through Fourier transform infrared (FTIR) spectroscopy to evaluate the reactive clusters existing on the surface. Utilizing a Perkin Elmer FTIR spectrometer (Spectrum IR version 10.6.2) in attenuated total reflection (ATR) mode, the different line of FTIR spectra were obtained. These measurements were executed at ambient temperature (25 °C) across a wavenumber interval of 4000 to 400 cm^{-1}. An examination via X-ray diffraction (XRD) was employed on powdered samples of KOH-based activated carbon using a Rigaku Diffractometer. The XRD instrument was set at 40 kV and 40 mA with a CuKα radiation (λ = 1.54059 Å). Recording of XRD patterns occurred at a speed of 3° per minute within a 2θ span of 10-90°. The surface characteristics and elemental alignment of the activated carbon were scrutinized through a field emission scanning electron microscope (FESEM, JEOL/FE version-2 instrument JSM-IT 800, USA). An in-depth surface investigation was performed using transmission electron microscopy (TEM) fortified with energy-dispersive X-ray spectroscopy (EDX) and additional components, particularly the Model-TALOSF200G2 by Thermo Fisher Scientific USA. The iodine number (IN) was determined to assess the micro-porosity of the carbon materials. The procedure involved adding a 5 % HCl solution (5 mL) to the carbon sample (1 g), boiling the mixture for 30 minutes, and then freezing it. Finally, 0.1 N, 10 mL iodine solution was added. After that the mixture was vigorously stirred for 1 minute before filtration and washed with distilled water. The filtrate was titrated with a sodium thiosulfate solution (0.1 N) by means of starch as an indicator, and the IN was calculated via formula,

$$IN = \frac{\text{weight of iodine adsorbed on carbon (mg)}}{\text{weight of carbon (g)}} \quad (1)$$

The methylene blue numeral (MBN) was determined to provide insights into the meso-porosity of the materials. It was determined by mixing the carbon sample (100 mg) with a methylene blue solution (75 mL, 1000 ppm) and stirring at 200 rpm for 3 hours at 25°C. After filtration, the remaining methylene blue concentration in the solution was measured by means of a UV-visible spectrophotometer at 665 nm. The MBN was then calculated as the maximum amount of dye adsorbed per gram of adsorbent, using the equation (2).

$$MBN = \frac{(C_0 - C_e) \times V}{m} \quad (2)$$

Where C_0 is the preliminary concentration, C_e is the equilibrium concentration, V is the volume of the solution, and m is the frame of the carbon.

2.3 Electrochemical characterization

The electrochemical characterization of the sample was carried out utilizing various methodologies, which included Cyclic Voltammetry (CV), Galvanostatic Charge Discharge (GCD), and Electrochemical. Impedance Spectroscopy (EIS) in order to elucidate the electrochemical properties inherent to it. These evaluations were executed using a Corrtest CS350 electrochemical workstation utilizing a three-electrode cell setup. The active material was applied onto nickel foam substrates, which were subsequently integrated into the electrochemical testing arrangement. An electrode featuring mercury/mercury oxide attended as the reference electrode and was immersed in a 3 M KOH, while a platinum wire (with theoretically higher capacitance compared to biomass derived activated carbon) was utilized as the counter electrode [18]. This meticulously prepared electrode was employed for ensuing electrochemical analyses. Cyclic Voltammetry (CV) and Galvanostatic Charge Discharge (GCD) assessments were performed across a potential range of -1 to 0 V, with diverse scan rates, to comprehensively evaluate the capacitive behavior of the material. The specific capacitance of the activated carbon electrode was evaluated from galvanostatic charge-discharge curve using the equation (3)

$$C_{sp} = \frac{I \times \Delta t}{m \times \Delta v} \quad (3)$$

Where I is the charge-discharge current, Δt is the discharge time in seconds, m is the active mass of activated carbon loaded on Ni-foam, and Δv is the potential window in volts.

3 Results and discussion

The lignocellulosic components present in the bark of *Acacia catechu* show a crucial part in the synthesis of the activated carbon at elevated temperatures. The chemical action of activating agent, KOH, enhances the porosity of the materials through its dehydrating action. The elevated temperature treatment significantly augments the degree of micro and mesoporosity within the carbon matrix, creating a hierarchical porous network [24]. This multi-channeled network, generated during the combined physical and chemical activation process, facilitates the efficient transmission of ions or charges, thereby enhancing the electrochemical concert of the activated carbon. To characterize the structural, morphological, and electrochemical.characteristics of the activated carbon, the following analytical techniques were employed:

3.1 Fourier transform infrared (FT-IR) spectroscopy

FTIR study techniques are employed to analyze functional groups present in the samples. The absence of significant peaks in all samples except in KBAC-0 specified that activated carbons were primarily composed of carbon structures. The FTIR spectrum is depicted in Fig. 2 (a). All KBAC-4, KBAC-6 and KBAC-8 samples exhibited distinguishing bands at 1603 cm^{-1}, 938 cm^{-1} and 864 cm^{-1}, accredited to the -C=C-, -C-H (bending) and $=CH_2$ (out of plane bending) functionalities, correspondingly. Around 1600-1700 cm^{-1} peak of C=O group from lignocellulose was observed. The bands observed at 2273 and 1098 cm^{-1} resemble to the –C=C-. Particularly, the prominent band around 2754 cm^{-1} corresponding to –OH group exhibited in FTIR spectra of KBAC-0 started to disappear along with the heat treatment (in KBAC-4) and did not appear in KBAC-6 and KBAC-8. In the FTIR spectrum of KBAC-8, significant peaks in the 800 to 1650 cm^{-1} region were observed with sp^2 hybridized –C=C bonds. The presence of aromatic and aliphatic –C=C– bonds suggests the graphitization of the carbon materials as a purpose of the elevated temperature [25]. The graphitization of the carbon materials was also supported by XRD analysis.

3.2 X-ray diffraction (XRD) characterization

The segment purity and crystallinity of KOH-activated carbon were assessed through X-ray diffraction (XRD) analysis. The diffraction patterns confirmed the phase purity of the samples, revealing broad peaks characteristic of carbon materials and no residual KOH, indicating the formation of pure carbon. The XRD patterns, observed under 2θ range from 10° to 90°, for KBAC-0, KBAC-4, KBAC-6 and KBAC-8 are illustrated in Fig. 2 (b). Remarkably, all the samples exhibited broad and sharp peaks, with a prominent broad peak at $2\theta \approx 26.8°$ equivalent to 0.33 nm d-spacing value and (002) plane, indicative of the graphitic nature of the carbon materials [8] which is consistent with FTIR result.

3.3 Raman spectroscopic study

Raman spectroscopic technique is employed to evaluate the vibrations due to presence of metals and graphitized carbon in the activated carbon. The examination was accompanied in the range of 100 to 3200 cm^{-1} using a wavelength of 514 nm. The Raman spectra of the all-activated carbon derived from the bark of *Acacia catechu* are presented in the Fig. 2 (c). The diagram depicted existence of two types of conspicuous broad peaks at 1335-1345 cm^{-1} and at 1580-1590 cm^{-1} ascribed to D-band (defect-induced mode) and G band (graphitic

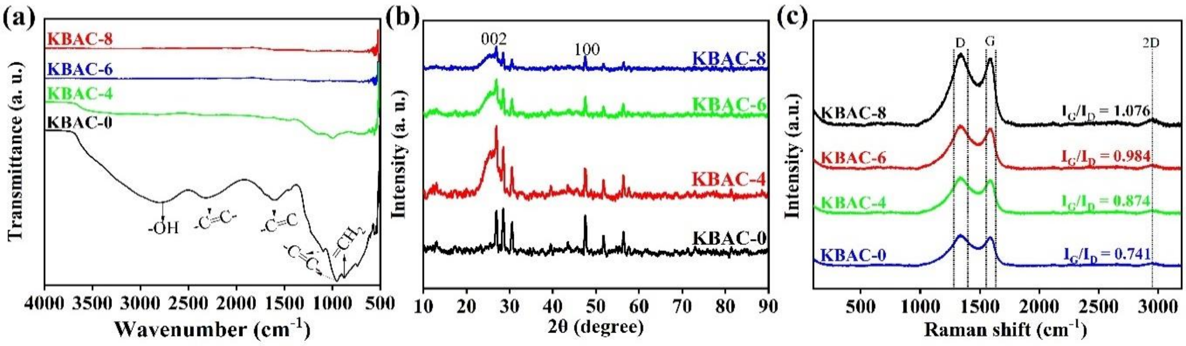

Fig. 2. (a) FTIR spectra (b) XRD patterns, and (c) Raman spectra of sample KBAC-0, KBAC-4, KBAC-6 and KBAC-8

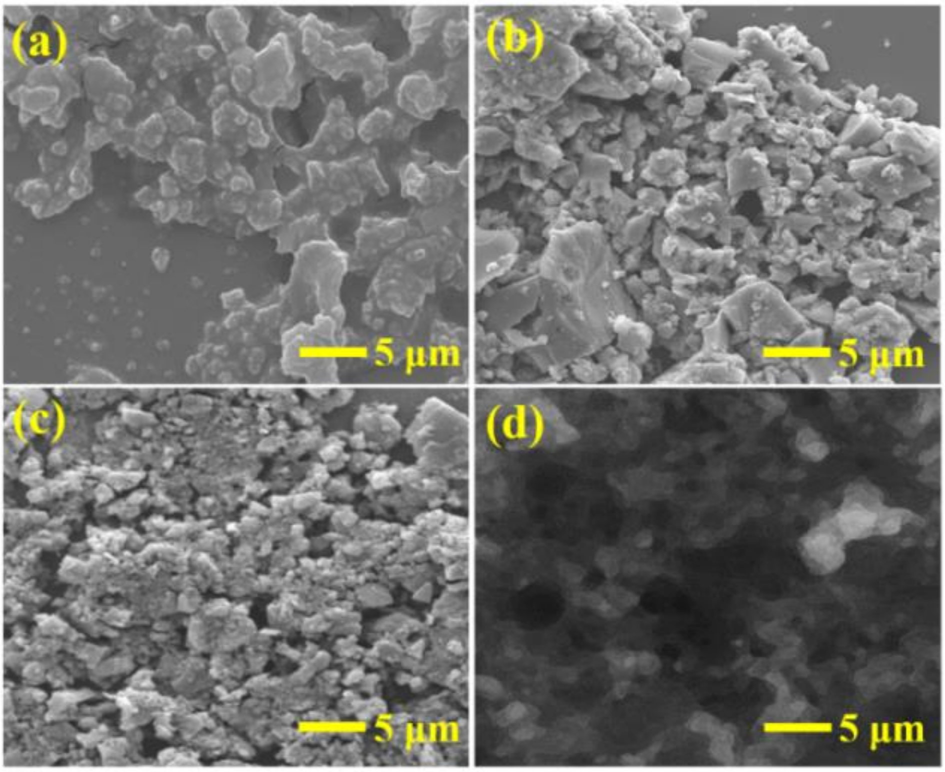

Fig. 3. FE-SEM image of (a) KBAC-0, (b) KBAC-4, (c) KBAC-6, and (d) KBAC-8 under magnification of 5 μm

e2g2 mode) correspondingly, characteristic of carbonaceous materials [26]. The ratio of G-band to the D-band (I_G/I_D) for sample KBAC-8 was found to be higher (1.076), clearly indicating the graphitic nature of the sample as function of temperature. The escalation in the I_G/I_D ratio with increasing carbonization temperature advocates a greater degree of graphitization due to higher structural disorder and defects in carbon matrix. Moreover, there is the presence of a 2D band at 2948 cm^{-1}, which is more pronounced on sample KBAC-8, indicating characteristic of graphene or other 2D materials [27]. This observed graphitic behavior is in accordance with the FTIR and XRD analyses, which collectively indicate the presence of graphitic structure in the material.

3.4 Field emission-scanning electron microscopy (FE-SEM) analysis

FE-SEM investigation provided insights into the three-dimensional morphology of the KBAC samples, revealing a porous structure conducive to ion and electron transport in high surface area platform. The FE-SEM images of KBAC-0, KBAC-4, KBAC-6 and KBAC-8 at a magnification of 5 μm are offered in Fig. 3 (a), (b), (c) and (d), correspondingly. The larger particles present in KBAC-0 fragmented to smaller ones due to thermal treatment under an inert atmosphere during the activation process, leading to a noteworthy intensification in the number of pores. This phenomenon is attributed to the thermal energy-induced degradation of the particle structure in the presence of an activating agent with release of gases, which ultimately contributes to the development of an interconnected porous network within the carbon material. The enhanced porosity, in turn, demonstrates enhanced specific capacitance of the materials, as it facilitates the efficient ions adsorption, desorption and channeling of the ions through the pores [19].

3.5 Iodine number (IN) and methylene blue number (MBN) method

The iodine and methylene blue number methods are widely used techniques for determining the micro-porosity and mesoporosity of activated carbon materials, respectively [8]. The bar graph of the samples demonstrating iodine number and methylene blue number is depicted in Fig. 4 (a) and (b), respectively. The iodine number method indicates that sample KBAC-0 exhibits a lower iodine number as well as methylene blue number. However, the sample activated at 800 °C displays a higher IN and MB number of 1371.41 mg/g and 205.61 mg/g, respectively. Overall results illustrate that an escalation in the activation temperature principals to an enhancement of micro and mesoporous structure within the carbon material [28].

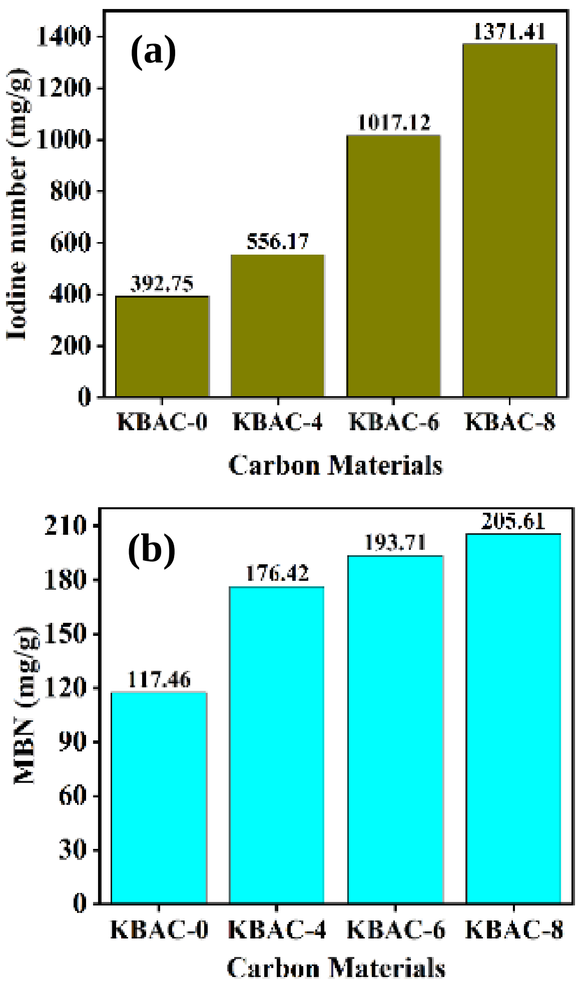

Fig. 4. Bar graph demonstrating (a) iodine number (IN) and (b) methylene blue number (MBN) of different carbon materials.

3.6 Transmission Electron Microscopy (TEM)

The structural orientation, crystalline properties, morphological distribution, and elemental constituent of the active carbon ingredients were examined by using TEM analysis. Selected area electron diffraction (SEAD) is a crystallographic experimental technique to study the diffraction pattern in TEM analysis. Fig. 5 (a, c, e, g) displays the SEAD pattern which exhibits a clear diffraction pattern of activated carbon. Fig. (b, d, f, h) depicts TEM image of KBAC samples. The TEM image of all samples reveals a smooth surface texture arising due to combined physical and chemical activation under elevated temperature. With the increase in temperature, the morphological modification occurs from smooth to rough surface, leading to the formation of the mesoporous surface with enhanced area and highly disordered carbon matrix [29]. The anisotropic nano-sized amorphous texture with mesophase characteristic of the KBAC-8 is attributed to the elevated temperature activation.

3.7 Electrochemical Characterization

A 3-electrode arrangement with a 3 M KOH was employed to measure the electrochemical data of the active material. The CV plot of sample KBAC-8 disclosed an almost rectangular form, which is indicative of the behavior of an electric double layer capacitor (EDLC) with prominent capacitive properties due to heat treatment. The other KBAC samples have lower area under the curve which is attributed to their less capacitive behavior. When a material undergoes a heat treatment at low temperatures, formation of pores within the material is suppressed or prevented which attributes to lower capacitance.

This form represents the electrolyte ions' reversible adsorption and desorption at the electrode-electrolyte interface, a characteristic of carbon-based electrode materials used in supercapacitors [30]. The comparative CV plot of all samples is illustrated in Fig. 6 (a).

The larger area under the CV curve for KBAC-8 compared to KBAC-6, KBAC-4 and KBAC-0 at 10 mV s^{-1}, suggests KBAC-8 possesses improved capacitive behavior. This can be attributed to the higher carbonization temperature, which enhances the porosity and surface area of the activated carbon, facilitating efficient ion adsorption and desorption at the interface of electrode and electrolyte. The absence of any redox peaks in the CV plots further confirms the EDLC nature of the activated carbon electrodes [6].

Fig. 7 (a), (c), (e) and (g) present the CV curves for samples KBAC-0, KBAC-4, KBAC-6 and KBAC-8, respectively, at various scanning rates from 5 to 150 mV s^{-1}. With the increasing scan rate, the area under the CV curve also increases, accompanied by a rise in current covering the more prominent area. The area under the curve is directly proportional to the charge passing during the electrochemical process in an effective double layer of charges. A larger area under the curve is a characteristic of effective double layers of charge including its capacitance and the surface area of the electrode. It means, a higher surface area in CV curve

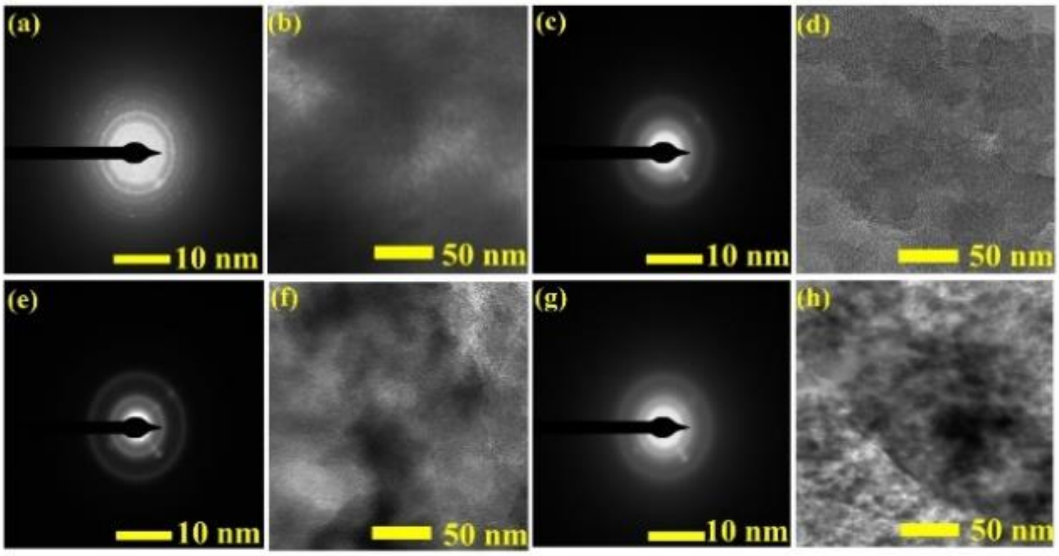

Fig. 5. SEAD and HR-TEM image of (a)-(b) KBAC-0, (c)-(d) KBAC-4, (e)-(f) KBAC-6, (g)-(h) KBAC-8, respectively.

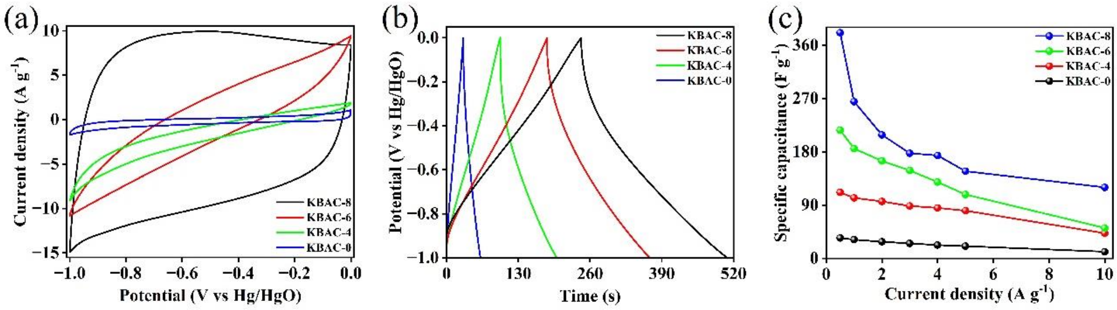

Fig. 6. Comparative illustration of (a) CV at 10 mV s^{-1} (b) GCD under 1 A g^{-1} (c) capacitance vs. current density for samples KBAC-0, KBAC-4, KBAC-6 and KBAC-8, respectively.

indicates a greater amount of charge transfer. In this context, materials with a higher surface area and uniform porous structure exhibit superior capacitive properties.

The GCD analysis provides a quantitative assessment of the energy storage capability of the activated carbon electrodes under various current densities (0.5 to 10 A g^{-1}). Fig. 6 (b) presents the comparative GCD plots of all KBAC samples at a current density of 1 A g^{-1}. The results clearly indicate that the KBAC-8 sample exhibits a longer discharge time compared to other counter KBAC samples, along with higher specific capacitance. The higher capacitance of KBAC-8 is due to the 3D nano-architectonics consisting of a number of mesopores and micropores contribute to better capacitive value through efficient transmission of ions within the carbon matrix [31,32].

The GCD plots of all samples unveil symmetrical triangular shapes as presented in Fig. 7 (b), (d), (f), and (h). The sample KBAC-8 exhibits specific capacitance of 380.81, 264.51, 208.44, 177.48, 173.72, 147.10, and 119.90 F g^{-1} at current densities of 0.5, 1, 2, 3, 4, 5, and 10 A g^{-1}, respectively. Gravimetric specific capacitance for KBAC-6, KBAC-4, and KBAC-0 are found to be 216.37, 185.38, 164.46, 148.32, 128.8, 107.85, and 51.30, 111.19, 102.13, 96.06, 88.35, 85.16, 80.50, 42.50 and 34.32, 31.52, 28.00, 25.26, 22.44, 20.60, 11.30 F g^{-1} under same current densities. In contrast, the KBAC-6 and KBAC-4 samples exhibit less linear charging-discharging plots with increased IR drop, likely due to reduced conductivity and electrode-electrolyte interaction. The interior resistance offered by the materials in the working electrode is escorted by the sharp IR drop during discharge, leading to depreciated specific capacitance at higher current densities [33]. KBAC-8 possess a larger reacting surface and activation sites for electron accumulation under confined areas, leading to better rate capability compared to KBAC-6 and KBAC-4. However, KBAC-0, due to non-optimal conditions for its preparation exhibits very low specific capacitance along with small rate capability. All in all, GCD plots reveal that high-temperature heat treatment or carbonization leads to the graphitization of carbon from sp^3 to sp^2 [34], which is also supported by FTIR and XRD spectra.

Fig. 8 (a), (b) and (c) illustrate the cyclic stability and Coulombic efficiency of samples KBAC-8, KBAC-6, and KBAC-4, respectively. The data reveals that KBAC-8 exhibits a higher capacity retention of 94.64% with outstanding Coulombic efficiency of 99.91% even subsequent 10,000 cycles of charging and discharging. This result supports the suitability of KBAC-8 as a superior electrode material.

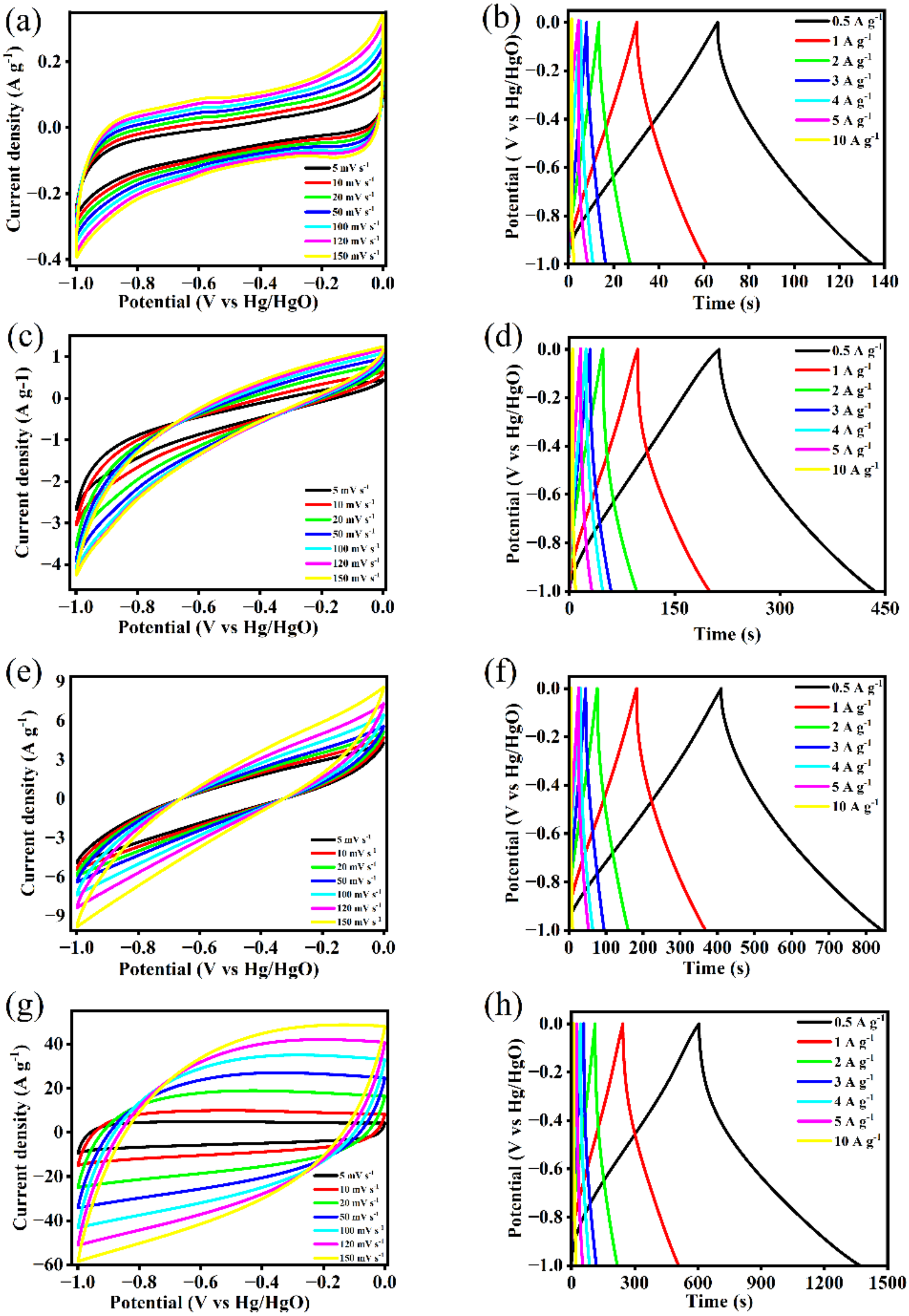

Fig. 7. (a), (c), (e) and (g) represent CV plot and (b), (d), (f) and (h) represent GCD of KBAC-0, KBAC-4, KBAC-6, and KBAC-8 respectively.

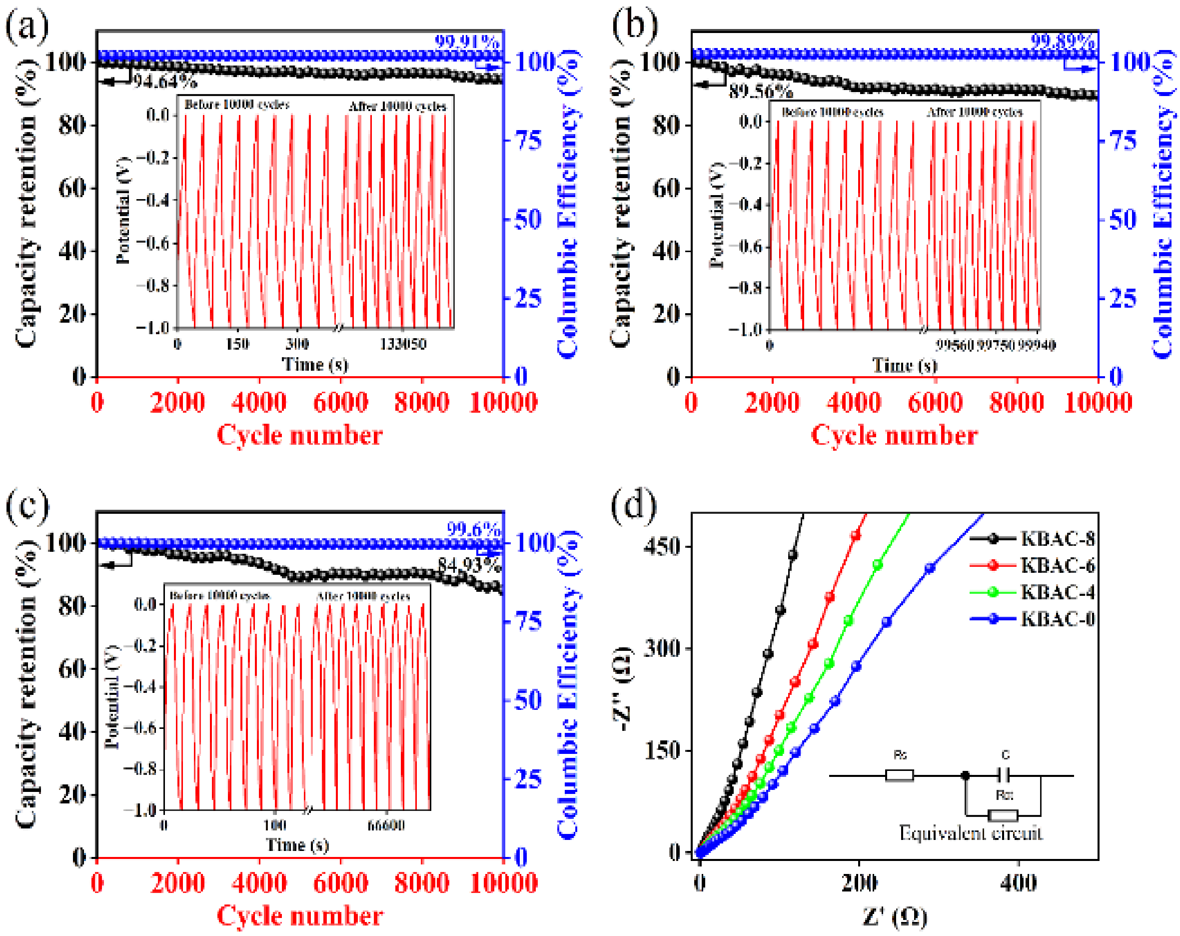

Fig. 8. Capacity retention and columbic efficiency of (a) KBAC-8, (b) KBAC-6, and (c) KBAC-4, respectively and each enclosure revealed GCD plot at 10 A g^{-1} before and after 10,000 charging-discharging cycles, (d) Nyquist plot of KBAC-8, KBAC-6, KBAC-4 and KBAC-0 samples with an equivalent circuit.

A comparative investigation of various biomass-derived activated carbons for supercapacitor applications discloses that the activated carbon derived from *Acacia catechu* bark exhibits astonishing potential as an electric double-layer capacitor (EDLC) electrode material. Its significantly higher specific capacitance with superior cyclic retention is particularly noteworthy, as it indicates the material's ability to maintain its performance over extended charge-discharge cycles. This property is crucial for the higher stability and reliability of supercapacitor devices [4].

The electron transfer kinetics of the working electrodes were measured over a frequency range spanning from 100 kHz to 1 mHz with an alternating current (AC) amplitude of 10 mV employing Electrochemical impedance spectroscopy (EIS). Nyquist plots of the KBAC samples are presented in Fig. 8 (d). The EIS spectra derived from the Nyquist plot can be characterized by presence of four distinct regions: (a) the electrolytic resistance (Rs), influenced by the ionic conductivity of the electrolyte and surface area of the electrode, (b) the semicircle segment adjacent to the x-axis, charge transfer resistance (Rct), which reflects impedance to ion/electron transfer between the electrolyte and the electrode, (c) the middle, somewhat horizontally inclined region demonstrating Warburg impedance (W), indicative of ion diffusion within the electrolyte, and (d) vertically inclined region at lower frequencies, exhibiting capacitive behaviour, attributed to the double layer capacitance at the interface [43]. The experimentally obtained EIS data was fitted using an equivalent circuit model, revealing that the KBAC-8 electrode exhibited lower resistive behavior compared to KBAC-6, KBAC-4, and KBAC-0. The Rct and Rs values for KBAC-8 got originated to be 0.73 Ω and 1.27 Ω, respectively, while for KBAC-6, KBAC-4 and KBAC-0 they were 0.87 Ω, and 2.36 Ω, 1.02 Ω, and 2.81 Ω and 1.28 Ω and 3.13 Ω, respectively (obtained from Zview software). The inferior Rct and Rs values of KBAC-8 indicate improved electron transfer kinetics and reduced internal resistance compared to other KBAC samples. This enhanced electrochemical performance of KBAC-8 can be accredited to its optimized porous structure and enhanced surface area, which facilitate efficient ion transport and adsorption, leading to superior capacitive behaviour and cycling stability. The comparative supercapacitive performance of biomass-derived carbon materials is summarized in Table 1.

The overall electrochemical performance of the activated carbon derived from the *Acacia catechu* bark in this research work is summarized in Table 2.

Table 1. Comparative overview of different carbon materials derived from biomass and the current research's applicability to supercapacitor applications.

S.N.	Source of biomass	Activating agent	Activation temperature (°C)	Maximum capacitance (F g^{-1})	Capacitance at current density	Electrolyte used	Cyclic Stability (cycles)	Reference
1	Areca nut midrib	KOH	800	192	1 Ag^{-1}	H_2SO_4	-	[35]
2	Lacquer wood	H_3PO_4	600	354	0.2 Ag^{-1}	1M H_2SO_4	95.3 (10000)	[36]
3	Corn husk	KOH	800	127	1 Ag^{-1}	6 M KOH	90% (5000)	[37]
4	*Camellia oleifera* Shells	$ZnCl_2$	600	266	0.2 Ag^{-1}	6 M KOH	91.3% (5000)	[38]
5	Agave leaves	K_2CO_3	800	205	5 mV s^{-1}	1M Na_2SO_4	-	[4]
6	Potato waste residue	$ZnCl_2$	700	255	0.5 Ag^{-1}	2 M KOH	93.7% (5000)	[39]
7	Sawdust	H_3PO_4	550	244.1	1 Ag^{-1}	1 M H_2SO_4	87% (10000)	[40]
8	Soybean	KOH	700	220	0.5 Ag^{-1}	6 M KOH	99.2% (10000)	[41]
9	*Citrus bergamia* peels	H_3PO_4	600	289	0.1 Ag^{-1}	6 M KOH	88% (5000)	[42]
10	*Acacia catechu* bark	KOH	800	264.51	1 A g^{-1}	3 M KOH	94.64 (10000)	This work

Table 2. Brief summary of outcomes of this research

S.N.	**Sample**	**IN (mg/g)**	**MBN (mg/g)**	**C_{sp} at 1 A g^{-1} (F g^{-1})**	**Retention (10000 cycles)**	**Rs (Ω)**	**Rct (Ω)**
1	KBAC-0	392.75	117.46	31.52	-	1.28	3.13
2	KBAC-4	556.17	176.42	102.13	84.93%	1.02	2.81
3	KBAC-6	1017.12	193.71	185.38	89.56%	0.87	2.36
4	KBAC-8	1371.41	205.61	264.51	94.64%	0.73	1.27

4 Conclusions

Nanoporous activated carbon was successfully synthesized in this study by utilizing waste bark sourced from Acacia catechu, employing a straightforward chemical activation technique with KOH as the activating agent. The characterization of the resulting activated carbon materials was conducted comprehensively through FTIR, XRD, SEM, TEM, iodine number, and methylene blue number analyses. An evaluation of the electrochemical recital of the activated carbon samples was carried out using a 3-electrode configuration. Through comparative analysis, it was observed that the KBAC-8 sample exhibited a significantly higher gravimetric capacitance of 264.51 F g-1 at 1 A g-1, along with lower resistive properties compared to the KBAC-6 sample, which displayed a capacitance of 185.38 F g-1 under the same current density. The exceptional supercapacitive characteristics of the KBAC-8 sample can be endorsed to the development of micro and mesopores on the activated carbon surface. This optimized porous structure facilitated effective ion transport and adsorption, ultimately resulting in improved electrochemical performance. In conclusion, the findings indicate that the KBAC-8 sample, with its favourable capacitive behaviour and minimal resistive features, holds promise as a promising material for utilization as a negatrode material in energy harvesting purposes.

The authors would like to acknowledge the university grants commission (UGC), Nepal for partial financial provision for this work.

References

1. Shrestha, R. L. *et al.* Washnut seed-derived ultrahigh surface area nanoporous carbons as high rate performance electrode material for supercapacitors. *Bull. Chem. Soc. Jpn.* **94**, 565–572 (2021).
2. Yin, Y. *et al.* Recent Progress and Future Directions of Biomass-Derived Hierarchical Porous Carbon : Designing , Preparation , and Supercapacitor Applications. (2023) doi:10.1021/acs.energyfuels.2c04093.
3. Dhakal, G. *et al.* High-performance supercapacitors fabricated with activated carbon derived from lotus calyx biowaste. *Renew. Energy* **189**, 587–600 (2022).
4. Lobato-Peralta, D. R. *et al.* Activated carbons obtained by environmentally friendly activation using solar energy for their use in neutral electrolyte supercapacitors. *J. Energy Storage* **52**, (2022).
5. Puziy, A. M., Poddubnaya, O. I., Martínez-Alonso, A., Suárez-García, F. & Tascón, J. M. D. Synthetic carbons activated with phosphoric - Acid I. Surface chemistry and ion binding properties. *Carbon N. Y.* **40**, 1493–1505 (2002).
6. Awasthi, G. P. *et al.* Synthesis and characterizations of activated carbon from Wisteria sinensis seeds biomass for energy storage applications. *J. Ind. Eng. Chem.* **72**, 265–272 (2019).
7. Mensah-Darkwa, K., Zequine, C., Kahol, P. K. & Gupta, R. K. Supercapacitor energy storage device using biowastes: A sustainable approach to green energy. *Sustain.* **11**, (2019).
8. González-García, P. Activated carbon from lignocellulosics precursors : A review of the synthesis methods , characterization techniques and applications. *Renew. Sustain. Energy Rev.* 1–22 (2017) doi:10.1016/j.rser.2017.04.117.
9. Liang, K. *et al.* Post-modified biomass derived carbon materials for energy storage supercapacitors: a review. *Sustain. Energy Fuels* **7**, 3541–3559 (2023).
10. Shrestha, R. L. *et al.* Nanoporous Carbon Materials Derived from Washnut Seed with Enhanced Supercapacitance. *Materials (Basel).* **13**, 1–13 (2020).
11. Pour, G. B., Fard, H. N., Aval, L. F. & Dubal, D. Recent advances in Ni-materials/carbon nanocomposites for supercapacitor electrodes. *Mater. Adv.* 6152–6174 (2023) doi:10.1039/d3ma00609c.
12. Yang, V. *et al.* Hierarchical porous carbon derived from jujube fruits as sustainable and ultrahigh capacitance material for advanced supercapacitors. *J. Colloid Interface Sci.* **579**, 347–356 (2020).
13. Najib, S. & Erdem, E. Current progress achieved in novel materials for supercapacitor electrodes: Mini review. *Nanoscale Adv.* **1**, 2817–2827 (2019).
14. Kayode, S. E. & González, F. J. Treatment of Biowaste for Electrodes in Energy Storage Applications: A Brief Review. *J. Compos. Sci.* **7**, (2023).
15. Anderson, B. D. & Tracy, J. B. Nanoparticle conversion chemistry: Kirkendall effect, galvanic exchange, and anion exchange. *Nanoscale* **6**, 12195–12216 (2014).
16. Patil, S. S. *et al.* Hybrid Solid State Supercapacitors (HSSC's) for High Energy & Power Density: An Overview. *Eng. Sci.* **12**, 38–51 (2020).
17. Wang, Y. *et al.* Biomass-based materials for advanced supercapacitor: principles, progress, and perspectives. *Aggregate* 1–20 (2023) doi:10.1002/agt2.428.
18. Yadav, N., Ritu, Promila & Hashmi, S. A. Hierarchical porous carbon derived from eucalyptus-bark as a sustainable electrode for high-performance solid-state supercapacitors. *Sustain. Energy Fuels* **4**, 1730–1746 (2020).
19. Neme, I., Gonfa, G. & Masi, C. Activated carbon from biomass precursors using phosphoric acid: A review. *Heliyon* **8**, e11940 (2022).
20. Ciftyurek, E. *et al.* Performance of activated carbons synthesized from fruit dehydration biowastes for supercapacitor applications. *Environ. Prog. Sustain. Energy* **38**, 0–2 (2019).
21. Adhikari, B., Aryal, B. & Bhattarai, B. R. A Comprehensive Review on the Chemical Composition and Pharmacological Activities of *Acacia catechu* (L.f.) Willd. *J. Chem.* **2021**, (2021).
22. Kumar, D., Thakur, C. L. & Bhardwaj, D. R. Biodiversity conservation and carbon storage of *Acacia catechu* willd . Dominated northern tropical dry deciduous forest ecosystems in north-western Himalaya : Implications of different forest management regimes. 1–16 (2022) doi:10.3389/fenvs.2022.981608.
23. Chen, W. *et al.* Insight into KOH activation mechanism during biomass pyrolysis: Chemical reactions between O-containing groups and KOH. *Appl. Energy* **278**, 115730 (2020).

24. Boundzanga, H. M. *et al.* Contributions of hemicellulose, cellulose, and lignin to the mass and the porous characteristics of activated carbons produced from biomass residues by phosphoric acid activation. *Biomass Convers. Biorefinery* **12**, 3081–3096 (2022).
25. Shrestha, D., Maensiri, S., Wongpratat, U., Lee, S. W. & Nyachhyon, A. R. Shorea robusta derived activated carbon decorated with manganese dioxide hybrid composite for improved capacitive behaviors. *J. Environ. Chem. Eng.* **7**, 103227 (2019).
26. Shrestha, K. R., Kandula, S., Kim, N. H. & Lee, J. H. A spinel MnCo2O4/NG 2D/2D hybrid nanoarchitectures as advanced electrode material for high performance hybrid supercapacitors. *J. Alloys Compd.* **771**, 810–820 (2019).
27. López-Díaz, D. *et al.* Towards understanding the Raman spectrum of graphene oxide: The effect of the chemical composition. *Coatings* **10**, 1–12 (2020).
28. Gnawali, C. L. *et al.* Nanoporous Activated Carbon Material from Terminalia chebula Seed for Supercapacitor Application. *C-Journal Carbon Res.* **9**, (2023).
29. Zhao, Z. *et al.* Lignosulphonate-cellulose derived porous activated carbon for supercapacitor electrode. *J. Mater. Chem. A* **3**, 15049–15056 (2015).
30. Li, S. *et al.* Investigation on pore structure regulation of activated carbon derived from sargassum and its application in supercapacitor. *Sci. Rep.* **12**, 1–17 (2022).
31. Apriwandi, A., Taer, E., Farma, R., Setiadi, R. N. & Amiruddin, E. A facile approach of micro-mesopores structure binder-free coin/monolith solid design activated carbon for electrode supercapacitor. *J. Energy Storage* **40**, 102823 (2021).
32. Cheng, P. *et al.* Biomass-Derived Carbon Fiber Aerogel as a Binder-Free Electrode for High-Rate Supercapacitors. *J. Phys. Chem. C* **120**, 2079–2086 (2016).
33. Ahmad, A. *et al.* Preparation and Characterization of Physically Activated Carbon and Its Energetic Application for All-Solid-State Supercapacitors: A Case Study. *ACS Omega* **8**, 21653–21663 (2023).
34. Jung, S. H. *et al.* Activated Biomass-derived Graphene-based Carbons for Supercapacitors with High Energy and Power Density. *Sci. Rep.* **8**, 1–8 (2018).
35. Yunita, A., Farma, R., Awitdrus, A. & Apriyani, I. The effect of various electrolyte solutions on the electrochemical properties of the carbon electrodes of supercapacitor cells based on biomass waste. *Mater. Today Proc.* (2023) doi:10.1016/j.matpr.2023.03.102.
36. Hu, S. C. *et al.* Structural changes and electrochemical properties of lacquer wood activated carbon prepared by phosphoric acid-chemical activation for supercapacitor applications. *Renew. Energy* **177**, 82–94 (2021).
37. Usha Rani, M., Nanaji, K., Rao, T. N. & Deshpande, A. S. Corn husk derived activated carbon with enhanced electrochemical performance for high-voltage supercapacitors. *J. Power Sources* **471**, 228387 (2020).
38. Zhang, J., Gong, L., Sun, K., Jiang, J. & Zhang, X. Preparation of activated carbon from waste Camellia oleifera shell for supercapacitor application. *J. Solid State Electrochem.* **16**, 2179–2186 (2012).
39. Ma, G. *et al.* Nitrogen-doped porous carbon derived from biomass waste for high-performance supercapacitor. *Bioresour. Technol.* **197**, 137–142 (2015).
40. Zhou, Y. *et al.* Sawdust-Derived Activated Carbon with Hierarchical Pores for High-Performance Symmetric Supercapacitors. *Nanomaterials* **12**, 810 (2022).
41. Jiao, S. *et al.* Nano-flower-like porous carbon derived from soybean straw for efficient N-S co-doped supercapacitors by coupling in-situ heteroatom doping with green activation method. *Appl. Surf. Sci.* **615**, 156365 (2023).
42. Gehrke, V. *et al.* Facile preparation of a novel biomass-derived H3PO4 and $Mn(NO_3)_2$ activated carbon from citrus bergamia peels for high-performance supercapacitors. *Mater. Today Commun.* **26**, (2021).
43. Zhang, Y. *et al.* Morphology-dependent $NiMoO_4$/carbon composites for high performance supercapacitors. *Inorg. Chem. Commun.* **111**, (2020).